

**Nonreflecting boundaries for ultrasound in fluctuating hydrodynamics of open systems**R. Delgado-Buscacioni<sup>1,\*</sup> and A. Dejoan<sup>2,†</sup><sup>1</sup>*Departamento Física Teórica de la Materia Condensada, Universidad Autónoma de Madrid, Campus de Cantoblanco, Madrid, E-28049, Spain*<sup>2</sup>*Departamento Energía, Unidad de Simulación Numérica y Modelización de Procesos, CIEMAT, Avenida Complutense 22 Edificio 20, 28040-Madrid, Spain*

(Received 11 April 2008; revised manuscript received 31 July 2008; published 27 October 2008)

We present a formulation for nonreflecting boundaries in fluctuating hydrodynamics. Nonreflecting boundary conditions are designed to evacuate sound waves out of the computational domain, thus allowing one to deal with open systems and to avoid finite size effects associated with periodic boundaries. Thermodynamic consistency for the fluctuation of the total mass and momentum of the open system is ensured by a fluctuation-dissipation balance which controls the amplitude of the sound waves generated by stress fluctuations near the boundary. We consider equilibrium and out-of-equilibrium situations (forced sound) in liquid water at ambient conditions and argon ranging from gas to liquid densities. Nonreflecting boundaries for fluctuating hydrodynamics make feasible simulations of ultrasound in microfluidic devices.

DOI: [10.1103/PhysRevE.78.046708](https://doi.org/10.1103/PhysRevE.78.046708)

PACS number(s): 47.11.-j, 47.35.Rs, 05.40.-a, 47.61.-k

**I. INTRODUCTION**

During the last decade interest in microfluidics has grown dramatically due to applications in industry. At these small scales, fluid flow can be described by *fluctuating hydrodynamics* [1] characterized by stress and heat flux fluctuations arising from the chaotic series molecular collisions underlying the coarse-grained hydrodynamic level [2]. Fluctuating hydrodynamics (FH) deals with small lumps of fluids (from micrometers to nanometers) so the generalization of the *non-reflecting boundary condition* (NRBC) presented here is meant to become a useful tool in simulations involving sound in nano and microfluidics. At such small wavelengths, sound waves oscillate at frequencies of the order of MHz-GHz, corresponding to the ultrasound regime. Ultrasound is used in a large list of technological and medical applications, which is still being explored. An interesting example is the possibility of producing devices to collimate sound [3], whose computational study clearly requires NRBCs. Another broad field of fundamental and technological interest is ultrasound-particle interaction, which is being used to characterize colloidal suspensions or to transport and manipulate nanoparticles [4]. Ultrasound-particle simulations are, however, scarce in the literature and have been limited to standing waves solved using periodic boundary conditions (PBC) via the lattice Boltzmann method (see, e.g., Ref. [5]).

In fact, fluctuating hydrodynamics has been so far applied using either rigid walls (RW) or PBCs, whereby the system folds to itself and no conditions are required at the boundaries. However, these kind of boundary conditions considerably limit the range of applications. When dealing with real devices one usually needs to consider general boundaries which enable one to “open up” one or several boundaries of the simulation domain. Open boundary conditions are usually required when one is interested in resolving the flow

within a part of the total system (a window); archetypal examples being the flow within a channel having a nonequilibrium pressure (or density) profile, plug flows, and shear flows. Also, simulations involving traveling waves require nonreflecting boundaries which enable one to evacuate sound out of the system. More generally, open boundaries can be used to impose far-field flow conditions which let vortices or heat travel outside the simulation window without reflection. A complete list of open boundary implementations can be found in Refs. [6,7]. While there has been considerable theoretical and numerical work on open boundary conditions in standard computational fluid dynamics (CFD) [8], including turbulent flow [9], to the best of our knowledge there has been no attempt to apply these ideas to fluctuating hydrodynamics. A key issue in fluctuating hydrodynamics is to take into account the exchange of mass, momentum, and energy between the open system and its surroundings. Such an exchange needs to be expressed in the form of a fluctuation-dissipation balance, ensuring that the variance of mass, momentum, and energy of the total (open) system satisfies the thermodynamic prescriptions.

In a more general context, flow-particle interactions are receiving a great deal of attention in several fields (and scales) ranging from an ensemble of particles in open turbulent flow to one single complex molecule in low Reynolds number flow. Consequently, computational methods designed to couple fluid and particle motion have been developed for different scenarios (such as turbulence, lattice Boltzmann [10], or fluctuating hydrodynamics codes [11]). The NRBC formulation allows one to extend the range of applications of these computational approaches. The present generalization of the method can be straightforwardly implemented in fluctuating lattice Boltzmann codes [12] and it might be inspiring for developing an improved open BC formulation for compressible turbulent flow. Nonreflecting boundaries for FH will also prove to be useful in hybrid schemes based on domain decomposition. An application is to embed a FH region of interest with a coarser and faster CFD (deterministic) scheme. The same idea applies for hybrid schemes designed to dynamically couple particle and

\*rafael.delgado@uam.es

†anne.dejoan@ciemat.es

continuum descriptions, such as direct simulation Monte Carlo (DSMC) [13] or molecular dynamics (MD) with FH [14,15]. These multiscale models enable one to solve fluid-particle interactions directly from the underlying solvent-solute molecular collisions, i.e., without assuming any phenomenological coupling law such as the Stokes force. Flux based hybrid methods can solve unsteady flow and have been applied to study the interaction between flow and complex molecules (such as polymers in flow [16,17] or sound waves against molecular assemblies [18]). In this context, the NRBC provides a natural way to evacuate sound waves out of the particle domain, through the open borders of the embedding hydrodynamic region.

In what follows we first present the fluctuating hydrodynamics equations, then, in Sec. III, we present the NRBC formalism. In Sec. IV we show that the only free parameter of the NRBC formulation can be evaluated from a fluctuation-dissipation balance which fits the variance of the total mass of the open system to its proper thermodynamic value. Section V presents results for the equilibrium state and nonequilibrium (forced waves) situations. Finally, conclusions are given in Sec. VI.

## II. FLUCTUATING HYDRODYNAMICS EQUATIONS

We shall focus on the treatment of open boundary conditions for sound waves in fluctuating hydrodynamics. Fluctuating hydrodynamics deals with flow within micron and sub-micron scales, and we shall consider sound waves with wavelengths of about  $\lambda \in [10-1000]$  nm, corresponding to frequencies in the MHz-GHz (ultrasound) regime. Due to its broad range of applications we consider water at ambient pressure and  $T=300$  K. The adiabatic constant (i.e., the specific heat ratio,  $\gamma=c_p/c_v$ ) of liquid water is almost unity ( $\gamma=1.0106$ ) so one can neglect the effect of temperature variations in the sound induced pressure fluctuations. We thus assume  $\gamma=1$ , which corresponds to a fluid with equal isothermal and adiabatic sound velocities. Sound propagates adiabatically and as in any adiabatic process, temperature and density fluctuations are related as  $(\partial p/\partial T)_\rho \delta T = (\gamma-1)(\partial p/\partial \rho)_T \delta \rho$ . Thus for  $\gamma=1$ , momentum and temperature equations are decoupled and sound is uniquely governed by mass and momentum equations.

We shall therefore consider the mass continuity and momentum equations for fluctuating hydrodynamics of a fluid with velocity components  $u_i$  ( $i=\{x,y,z\}$ ), density  $\rho$ , and fixed temperature  $T$ .

$$\frac{\partial \rho}{\partial t} + \frac{\partial \rho u_i}{\partial x_i} = 0, \quad (1)$$

$$\frac{\partial \rho u_i}{\partial t} + u_j \frac{\partial \rho u_i}{\partial x_j} = - \frac{\partial}{\partial x_j} (p \delta_{ij} + \Pi_{ij}), \quad (2)$$

where the right-hand side of Eq. (2) represents the full pressure tensor:  $p$  is the thermodynamic pressure and  $\Pi_{ij}$  is the stress tensor, which can be decomposed into a mean contribution  $\bar{\Pi}_{ij}$  and a fluctuating part  $\tilde{\Pi}_{ij}$ . The mean viscous tensor is given by

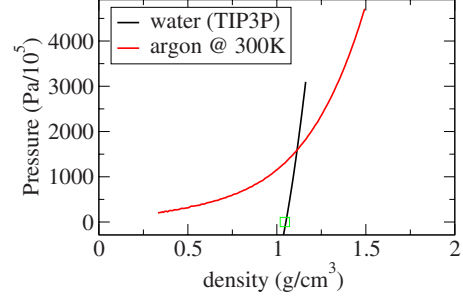


FIG. 1. (Color online) Pressure equation of state at  $T=300$  K for argon (Lennard-Jones model) and water (TIP3P model).

$$\bar{\Pi}_{ij} = - \left[ \eta \left( \frac{\partial u_i}{\partial x_j} + \frac{\partial u_j}{\partial x_i} - \frac{2}{3} \frac{\partial u_l}{\partial x_l} \delta_{ij} \right) + \xi \frac{\partial u_i}{\partial x_l} \delta_{lj} \right], \quad (3)$$

where  $\eta$  and  $\xi$  are, respectively, the longitudinal and bulk viscosities and summation is indicated over repeated subindexes.

The fluctuating tensor is written according to Serrano and Español [19],

$$\tilde{\Pi}_{ij} = A \left[ \frac{dW_{ij} + dW_{ji}}{2} - \frac{dW_{ll}}{3} \right] + B \frac{dW_{ll}}{3}, \quad (4)$$

where  $dW_{ij}$  is a random matrix of unit variance and the coefficients  $A$  and  $B$  are given by

$$A = \left( 4k_b T \frac{\eta}{V_c} \right)^{1/2}, \quad (5)$$

$$B = \left( 2Dk_b T \frac{\xi}{V_c} \right)^{1/2}, \quad (6)$$

where  $k_b$  is the Boltzmann's constant,  $V_c$  is the cell volume, and the spatial dimension is  $D=3$ .

The covariance of the random stress is given by

$$\langle \tilde{\Pi}_{ij}(x,t) \tilde{\Pi}_{kl}(x',t') \rangle = \frac{2k_b T}{V_c} \left[ \eta \left( \delta_{ik} \delta_{jl} + \delta_{il} \delta_{jk} - \frac{2}{3} \delta_{ij} \delta_{kl} \right) + \xi \delta_{ij} \delta_{kl} \right] \delta(x-x') \delta(t-t'), \quad (7)$$

so that the correlation of the longitudinal components are

$$\langle \tilde{\Pi}_{xx}(x,t) \tilde{\Pi}_{xx}(x',t') \rangle = \frac{2k_b T}{V_c} \left( \frac{4}{3} \eta + \xi \right) \delta(x-x') \delta(t-t'). \quad (8)$$

The equations of continuity and momentum are completed by the equations of state  $p=p(\rho, T)$  and the constitutive relations for the shear and bulk viscosity  $\eta=\eta(\rho, T)$  and  $\xi(\rho, T)$ , respectively. As stated we considered water at  $T=300$  K and ambient pressure. The equation of state  $p=p(\rho)$  and viscosities corresponds to the TIP3P water model at  $T=100$  K used in MD and obtained in a previous work [20] (see Fig. 1). In order to test the model against a broader range of thermodynamic and fluid conditions we also considered argon at several densities and temperatures (see Ref. [21] and Fig. 1 for the equation of state and [22] for viscosi-

ties). The adiabatic constant of argon is larger than one ( $\gamma \simeq 1.5$ ) so in assuming  $\gamma=1$  we underestimate the sound velocity of argon. However, in doing so, neither the physics of sound nor the open boundary model are essentially altered (see Sec. III C).

### III. NONREFLECTING OUTFLOW BOUNDARY CONDITIONS

Open boundary conditions are needed in most practical cases involving fluid dynamics processes. To that end Poinot and Lele [6] derived the Navier-Stokes characteristic boundary conditions (NSCBCs) procedure for deriving different kinds of boundary conditions in computational fluid dynamics from physical grounds. The central idea is to use relations based on the analysis of the different waves crossing the boundaries of the computational domain. The NSCBC method is an extension of the Euler characteristic boundary condition methodology used for specifying boundary conditions in hyperbolic systems (Euler equations) [23,24]. Our main purpose here is to apply the NSCBC approach to obtain nonreflecting boundary conditions (NRBCs) for an open fluctuating hydrodynamics system.

#### A. General formulation

Following the characteristic analysis [24] for waves propagating in the (normal to boundary)  $x$  direction, we recast the Navier-Stokes equations [Eqs. (1) and (2)] in the following form:

$$\frac{\partial \rho}{\partial t} + \frac{1}{c^2} \left[ L_2 + \frac{1}{2}(L_5 + L_1) \right] + \frac{\partial \rho v}{\partial y} + \frac{\partial \rho w}{\partial z} = 0, \quad (9)$$

$$\begin{aligned} \frac{\partial \rho u}{\partial t} + u \frac{1}{c^2} [L_2 + (L_5 + L_1)] + \frac{1}{2c} (L_5 - L_1) + \frac{\partial \rho v u}{\partial y} + \frac{\partial \rho w u}{\partial z} \\ = - \frac{\partial \Pi_{xx}}{\partial x} - \frac{\partial \Pi_{xy}}{\partial y} - \frac{\partial \Pi_{xz}}{\partial z}, \end{aligned}$$

$$\begin{aligned} \frac{\partial \rho v}{\partial t} + v \frac{1}{c^2} [L_2 + (L_5 + L_1)] + \rho L_3 + \frac{\partial \rho v v}{\partial y} + \frac{\partial \rho w v}{\partial z} \\ = - \frac{\partial \Pi_{yx}}{\partial x} - \frac{\partial \Pi_{yy}}{\partial y} - \frac{\partial \Pi_{yz}}{\partial z}, \end{aligned} \quad (10)$$

where  $u$ ,  $v$  are fluid velocities along  $x$  and  $y$  directions [ $i = 1, 2$  in Eqs. (1) and (2)]; the equation for  $w$ , in the  $z$  direction is similar to  $v$  and has been omitted. The  $L_i$ 's are given by [24]

$$L_1 = \lambda_1 \left( \frac{\partial p}{\partial x} - \rho_e c \frac{\partial u}{\partial x} \right), \quad (11)$$

$$L_2 = \lambda_2 \left( c^2 \frac{\partial \rho}{\partial x} - \frac{\partial p}{\partial x} \right), \quad (12)$$

$$L_3 = \lambda_3 \frac{\partial v}{\partial x}, \quad L_4 = \lambda_4 \frac{\partial w}{\partial x}, \quad (13)$$

$$L_5 = \lambda_5 \left( \frac{\partial p}{\partial x} + \rho_e c \frac{\partial u}{\partial x} \right), \quad (14)$$

and  $\lambda_i$  are the characteristic velocities

$$\lambda_1 = u - c,$$

$$\lambda_2 = \lambda_3 = \lambda_4 = u,$$

$$\lambda_5 = u + c. \quad (15)$$

Here  $\lambda_1$  and  $\lambda_5$  are the propagative velocities of sound waves moving in the negative and positive  $x$  directions and  $\lambda_2$ ,  $\lambda_3$ , and  $\lambda_4$  correspond respectively, to the advection velocity of entropy and transversal velocities  $v$  and  $w$ , along the  $x$  direction.

The set of open boundary conditions are obtained from Eqs. (9) and (10) by neglecting the transverse terms ( $\partial \cdot / \partial y$ ,  $\partial \cdot / \partial z$ ). Using the continuity equation (9) into the momentum equation (10) one derives the following relations in terms of primitive variables [6]:

$$\frac{\partial \rho}{\partial t} + \frac{1}{2c^2} (L_5 + L_1) = 0, \quad (16)$$

$$\frac{\partial p}{\partial t} + \frac{1}{2} (L_5 + L_1) = 0, \quad (17)$$

$$\frac{\partial u}{\partial t} + \frac{1}{2\rho_e c} (L_5 - L_1) = - \frac{1}{\rho_e} \frac{\partial \Pi_{xx}}{\partial x}, \quad (18)$$

$$\frac{\partial v}{\partial t} + L_3 = - \frac{1}{\rho_e} \frac{\partial \Pi_{yx}}{\partial x}. \quad (19)$$

Where  $\rho_e$  is the equilibrium density. As stated in this work we focus on sound waves and shall not consider heat transport. This implies that pressure and density perturbations are proportional to each other,  $\delta p = c^2 \delta \rho$  and  $L_2 = 0$ . Equation (9) simplifies to Eq. (16), which is redundant with Eq. (17). Also, transverse flow (shear) is zero,  $v = w = 0$ , so that  $L_3 = L_4 = 0$ . A general (deterministic) formulation considering the full set of hydrodynamic modes and several kinds of implementations of the NSCBC can be found in Refs. [6,7].

Linear hydrodynamics of a monocomponent fluid along one direction ( $x$ ) can be expressed in terms of five *characteristic waves*  $A_i$  (also called normal or hydrodynamic modes [25]). These are, namely, two sound waves traveling in opposite senses ( $A_1$  and  $A_5$ ), one heat wave ( $A_2$ ), and two shear waves ( $A_3$  and  $A_4$ ) in the transverse directions. In particular, the amplitude of the sound waves  $A_1$  and  $A_5$  is given in terms of the pressure and velocity perturbations with respect to equilibrium:  $\delta p = p - p_e$  and  $\delta u = u - u_e$  (here  $u_e = 0$ ),

$$A_1 = \frac{1}{2} \left( \frac{\delta p}{\rho_e c} - \delta u \right) \quad \text{wave moving } \leftarrow, \quad (20)$$

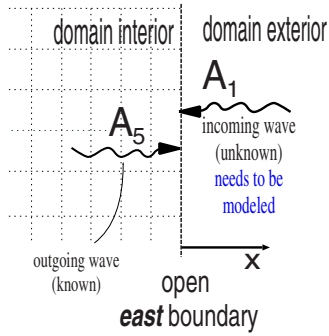


FIG. 2. (Color online) Incoming and outgoing sound waves through the east boundary.

$$A_5 = \frac{1}{2} \left( \frac{\delta p}{\rho_e c} + \delta u \right) \quad \text{wave moving } \rightarrow . \quad (21)$$

Introducing the definitions (20) and (21) into Eqs. (17) and (18) and considering the inviscid limit, one obtains that  $\partial A_i / \partial t + \lambda_i \partial A_i / \partial x = 0$ , meaning that  $A_i$  are conserved along the characteristic line  $x + \lambda_i t = \text{constant}$  (in the inviscid limit  $A_1$  and  $A_5$  are called the Riemann acoustic invariants). A clear physical insight of the operators  $L_i$ 's defined in Eqs. (11)–(14) can now be given by noting that (in the inviscid limit)  $\partial A_i / \partial t = -L_i / (2\rho_e c)$ . Thus  $L_i$  is proportional to the characteristic wave intensity (and  $2\rho_e c$  is sometimes called acoustic impedance, by analogy with the electrodynamics relation). In the viscous case one gets

$$\frac{\partial A_i}{\partial t} + \frac{L_i}{2\rho_e c} = \pm \frac{1}{2\rho_e} \frac{\partial \Pi_{xx}}{\partial x}, \quad (22)$$

where the sign  $+$  at the left hand side of the equation corresponds to  $A_1$  (sign  $-$  to  $A_5$ ).

The NSCBC approach is to infer values for the wave amplitude variations from the local (near to boundary) characteristic waves traveling across the *normal-to-boundary* direction ( $x$ ). To that end, the NSCBC approach relies on the determination of the  $L_i$ 's at (or near) the boundary. In principle, one can use Eqs. (11)–(14) to calculate  $L_i$  from the local gradients of pressure and velocity. However, one needs to distinguish the sense of the wave propagation required for this evaluation. In particular,  $L_1$  is associated to waves propagating leftwise in  $x$  direction (while  $L_5$  corresponds to waves moving rightwise). Hence, if for example, we consider the east boundary of a one-dimensional (1D) domain:  $A_5$  is a wave moving outwards, but within the domain, while  $A_1$  moves inwards, coming from outside. Thus, while  $L_5$  can be estimated using the pressure and velocity at interior points, to guess  $L_1$  one needs some extra information (some condition at the exterior). This guess is one of the essential tricks of the trade. In the foregoing discussion, for the sake of clarity, we shall always consider the east boundary so that  $L_5$  is associated to outgoing waves and  $L_1$  to incoming waves, as illustrated in Fig. 2.

Once the  $L_i$ 's are known, Eqs. (16)–(19) are then used to compute all other variables required at the boundary. This last step requires boundary conditions for the viscous terms involving normal derivatives to the boundary. According to

the theoretical results of Strikwerda [26] and Olinger and Sundstrom [27] one usually imposes weak viscous conditions at the border. In practice this means a vanishing normal stress  $\partial \Pi_{xx} / \partial x = 0$ , in the right-hand side of Eq. (18). The validity of this approximation, known as the *local one-dimensional inviscid* (LODI) problem [8], is justified by Poinso and Veynante [7]: viscous terms are already explicitly solved everywhere inside the domain, so the amplitude  $L_5$  (which is measured *inside*) already contains viscous effects. In agreement with this statement, we tested Eq. (18) with and without the viscous term and found similar outcomes.

### B. Nonreflecting outflow at fixed pressure

The natural choice for building a nonreflecting outlet condition according to the NSCBC approach would be to impose the amplitude variation of the incoming wave  $L_1$  to zero,  $L_1 = 0$ . However, this condition leads to large drift of the mean pressure. Physically, a perfectly nonreflecting boundary condition can be ill posed. Indeed, the information on the mean pressure is conveyed by waves reflected into the domain from the outside flow (where the static pressure  $p_\infty$  at infinity, or equivalently, the equilibrium pressure  $p_e = p_\infty$  is specified). If the local pressure  $p$  at the outlet is different from  $p_e$ , a reflected wave should be produced to bring  $p$  closer to  $p_e$ . With perfectly nonreflecting boundary conditions ( $L_1 = 0$ ) this information is not fed back into the computation domain. It is on this physical ground that Rudy & Strikwerda [28] proposed to add information on the mean static pressure at infinity  $p_e$ , and write the amplitude of the incoming wave as follows:

$$L_1 = K(p - p_e) \quad \text{with} \quad K = \frac{\sigma c(1 - \mathcal{M}^2)}{L}, \quad (23)$$

where  $L$  is a characteristic length size of the domain,  $\mathcal{M} = u/c$  is the Mach number, and  $\sigma$  is a constant that has to be fixed. At a low Mach number, as those considered in this work, one can write  $K = \sigma c/L$ .

By inserting Eq. (23) into Eq. (17) in the absence of an outgoing wave ( $L_5 = 0$ ), one sees that the expression (23) can be interpreted as a corrective term that relaxes exponentially the pressure at the frontier to the equilibrium pressure  $p_e$ . The relaxation time is  $\tau \equiv 1/K = 2L/\sigma c$ . Some caution is necessary to estimate the value of the constant  $\sigma$  (see the next section): too low values of  $\sigma$  can produce large pressure drift resulting in nonconvergence of the calculations, while large values of  $\sigma$  lead to high reflection. Thus, the price one pays for the stability of the scheme is that Eq. (23) yields a partially nonreflecting boundary. This important drawback was recently put forward by Selle *et al.* [29] and Polifke *et al.* [30]. They proved that although the linear relaxation term (23) leads to an effective nonreflecting boundary for the high-frequency regime (i.e., for wave frequencies much larger than the decay rate  $K$ ), it becomes highly reflecting for the low-frequency range [31]. But in fact these long, low-frequency waves are precisely those one would like to evacuate, because they can travel over long distances before being damped by viscosity. In order to extend the nonreflecting

property of the boundary condition to the low-frequency range, Polifke *et al.* [30] proposed the following modification to  $L_1$ :

$$L_1 = K(p - \rho_e c A_5 - p_e). \quad (24)$$

This modification applies for plane acoustic waves with normal incidence to the boundary and it is referred to as “plane-wave masking.” It consists in removing the contribution of the outgoing waves  $A_5$  to the pressure  $p$  from the linear relaxation term  $L_1$  so that the (reflected) outgoing wave no longer contributes to the incoming wave  $A_1$ . In this way, the incoming wave  $A_1$  is built up to suppress (or to “mask”) any reflection contribution from the outgoing wave. The result is that, in practice,  $A_5$  leaves the domain without being reflected. Polifke *et al.* [30] considered acoustic waves in turbulent flow and argue that if deviations from the equilibrium pressure  $p_e$  were only caused by plane acoustic waves (i.e., in the absence of turbulent fluctuations), the use of Eq. (24) would lead to a vanishing reflection coefficient for plane harmonic waves of arbitrary frequency. However, the results of this work for the (nonturbulent) deterministic regime (i.e., without fluctuations) coincide with those reported in their work [30]. This indicates that the partial reflection observed at short wavelengths [ $\lambda/\Delta x < 10$  (see Sec. V C)] is, in fact, related to numerical resolution. Also in the fluctuating hydrodynamics context, Eq. (24) is the best choice to evacuate most waves ( $\lambda/\Delta x > 10$ ) out of the system, as it provides the lowest reflection coefficient.

We now provide more insight into the incoming wave amplitude  $L_1$  proposed in Eq. (24). By using the definition of  $A_5$  in Eq. (21) and the definition of  $A_1$  given by Eq. (20) one gets

$$L_1 = \frac{K}{2}(\delta p - \rho_e c \delta u) = K \rho_e c A_1. \quad (25)$$

Using Eq. (22) one gets the following equation for  $A_1$ :

$$\frac{\partial A_1}{\partial t} + K' A_1 = \frac{1}{2\rho_e} \frac{\partial \Pi_{xx}}{\partial x} \quad \text{with } K' = K/2. \quad (26)$$

Equation (26) sheds more light on how the plane-wave masking controls the incoming waves. In the inviscid limit, the solution of Eq. (26) is simply an exponential decay  $A_1 \sim \exp(-K't)$ . Hence, the incoming waves are damped at a rate  $K'$ . In fact, by damping the incoming wave to its equilibrium value  $\langle A_1 \rangle = 0$ , one also controls the deviation from the equilibrium pressure, which relaxes to  $\langle \delta p \rangle = 0$ . By comparison, as stated above, Eq. (23) is only designed to control the overall pressure drift, but not the amplitude of the incoming wave.

It is important to highlight that in the case of fluctuating hydrodynamics, Eq. (26) also acts as a source of incoming random waves. Indeed, the local fluctuating stress near the border is a source of white noise which triggers waves into the system. The boundary condition given in Eq. (26) determines the resulting spectra for the amplitude of incoming waves: at equilibrium the time correlation of incoming waves is a colored noise,  $\langle A_1(t)A_1(0) \rangle \propto \exp(-K't)/K'$ , and

their power spectral density is proportional to  $S_{A_1}(\omega) \propto 1/(\omega^2 + K'^2)$ . Implications of this fact are discussed in Sec. IV.

### C. Fluctuation-dissipation balance

In previous works the relaxation time  $1/K$  was set proportional to the inverse of sound time over a distance  $L/\sigma$ , i.e.,  $1/K = L/(\sigma c)$ . The constant  $\sigma$  was set according to numerical “optimization” but not based on physical grounds. For instance, when making use of expression (23) for  $L_1$ , estimations of the optimal value of  $\sigma$  by Rudy and Strikwerda, provided  $\sigma = 0.58$ , while Selle *et al.* [29] suggest  $0.1 < \sigma < \pi$ . By contrast, by making use of Eq. (24) for  $L_1$ , Polifke *et al.* [30] report  $\sigma = 167$  as the minimum value required to avoid pressure drift in their computations of a fully developed turbulent channel flow. In this work we address this problem from the perspective of fluctuating hydrodynamics and provide a route to estimate a value of  $K$  with physical content. The overall mass is governed by the amplitude of the incoming waves, so that by imposing the correct variance to  $A_1$ , one should get the correct variance for the total mass in the system. To that end, we consider the fluctuation-dissipation (FD) balance for the amplitude of the incoming waves  $A_1$  in the equilibrium state. We believe that the method proposed here below could be applied, for instance, to turbulent flow, provided there is some knowledge of the amplitude of fluctuations of  $A_1$  (i.e., of pressure and velocity) and of the stress tensor  $\Pi$ .

Let us consider Eq. (26) near the east boundary, in particular, at the cell face  $x_b = x_{f_{n-1}}$  where the NRBC is imposed (see Appendix B). We integrate Eq. (26) along a cell volume  $V_c = S\Delta x$  around the cell face  $x_b$  to get

$$\frac{dA_1(x_b)}{dt} + K' A_1(x_b) = F(t), \quad (27)$$

where we note that in the spirit of the finite volume method  $A_1(x_b) = (1/\Delta x) \int_{x_b - \Delta x/2}^{x_b + \Delta x/2} A_1(x) dx$ . The term  $F(t)$  in Eq. (27) acts as a random source which should be balanced with the damping term  $K' A_1$ . In deriving this balance we shall consider the random source  $F(t)$  arising from the random stress and omit its viscous part (note that amplitudes of viscous and random stresses are balanced by the fluctuating hydrodynamics formulation). This approximation permits us to close Eq. (27) and obtain an estimation of  $K$  which should, however, provide its proper functional dependence [32]. Spatial integration of the random stress in the right-hand side of Eq. (26) yields

$$F(t) \equiv \frac{1}{2\Delta x \rho_e} [\tilde{\Pi}_{xx}(x_b + \Delta x/2) - \tilde{\Pi}_{xx}(x_b - \Delta x/2)]. \quad (28)$$

Equation (27) is a stochastic differential equation which can be solved using standard techniques [33]. The noise source is coming from the local stress tensor, which at equilibrium satisfies [see Eq. (8)]

$$\langle \tilde{\Pi}_{xx}(t) \tilde{\Pi}_{xx}(0) \rangle = \frac{2k_B T \eta_L}{V_c} \delta(t), \quad (29)$$

where  $\eta_L = 4\eta/3 + \xi$ , is the longitudinal viscosity. Moreover, the fluctuating stress tensor is uncorrelated in space so the time correlation of the noise  $F(t)$  satisfies

$$\langle F(t)F(0) \rangle = 2\Phi \delta(t) = \frac{k_B T \eta_L}{\Delta x^2 \rho_e^2 V_c} \delta(t), \quad (30)$$

where the noise amplitude  $2\Phi$  is defined from the same equation (30). The fluctuation-dissipation balance, applied to Eq. (27), states that (see, e.g., [33])

$$\langle A_1^2 \rangle = \frac{\Phi}{K'}. \quad (31)$$

At equilibrium the variance of  $A_1$  can be obtained from standard thermodynamics. From Eq. (20)  $\langle A_1^2 \rangle = (1/4)[\langle \delta p^2 \rangle / (\rho_e c)^2 + \langle \delta u^2 \rangle]$ . But  $\langle \delta p^2 \rangle = c^4 \langle \delta \rho^2 \rangle$ ,  $\langle \delta \rho^2 \rangle = \rho_e k_B T / (c^2 V_c)$ , and  $\langle \delta u^2 \rangle = k_B T / (\rho_e V_c)$ , so one concludes that

$$\langle A_1^2 \rangle = \frac{1}{2} \frac{k_B T}{\rho_e V_c}. \quad (32)$$

Inserting Eqs. (32) and (30) into Eq. (31), one finally gets the decay rate  $K'$  or equivalently of  $K$  [see Eq. (26)],

$$K' = \frac{\nu_L}{\Delta x^2} \rightarrow K = \frac{2\nu_L}{\Delta x^2}, \quad (33)$$

where  $\nu_L = \eta_L / \rho_e$  is the kinematic longitudinal viscosity. The result contrasts with the form of  $K$  proposed in previous works ( $K = \sigma c / L$ ); in fact Eq. (33) shows no dependence with the sound velocity  $c$  or on the system size  $L$ . As stated, in this work we consider a fluid with adiabatic constant  $\gamma = 1$ , such as liquid water. However, we note that the derivation of Eq. (33) remains valid for arbitrary  $\gamma$  [34]. We note that for  $\gamma = 1$  the isothermal and adiabatic sound velocities coincide and one can neglect temperature effects on the sound waves while, for compressible fluids such as argon ( $\gamma > 1$ ), one needs to consider the energy equation to consistently solve sound. However, the inclusion of the energy equation in the present open boundary formalism does not require any extra (relaxation) parameter at the boundary. In fact the propagation of the heat mode across the boundary can be solved using the information *within* the computational domain (see Ref. [7]).

In Appendix B we present a numerical implementation of the plane-wave masking boundary conditions for a staggered grid, which ensures numerical stability for “open” fluctuating hydrodynamics.

#### IV. MASS FLUCTUATION AT EQUILIBRIUM

As stated above, by ensuring the fluctuation-dissipation balance for the amplitude of the incoming waves one expects to provide the correct variance of total mass, whose value at equilibrium is prescribed by thermodynamics. In particular, at equilibrium, the mass  $M(t)$  of an open system of volume  $V$  at temperature  $T$ , fluctuates with a variance given by

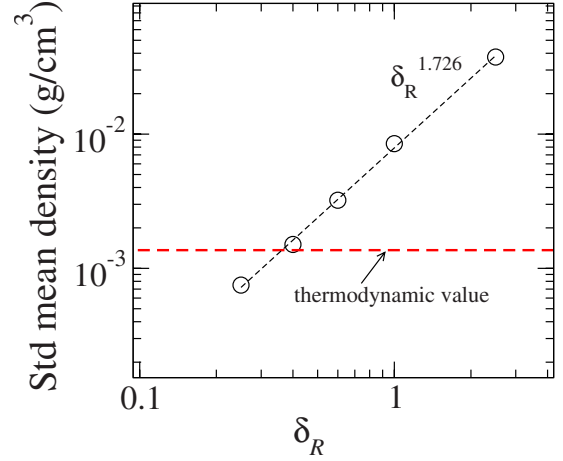


FIG. 3. (Color online) The standard deviation of the total mass in the simulation domain at equilibrium, versus the parameter  $\delta_R$ , which determines the relaxation rate  $K = \nu_L / (\delta_R \Delta x)^2$ . The dashed line is the thermodynamic prescription. At the optimum value  $\delta_R \approx 0.4$ , the variance of the overall mass coincides with the thermodynamic value.

$k_B T V / c^2$ , while the variance of the mean density  $\bar{\rho}(t) = M(t) / V$  is

$$\langle (\delta \bar{\rho})^2 \rangle = \frac{k_B T}{c^2 V}, \quad (34)$$

where  $\delta \bar{\rho} = \bar{\rho} - \rho_e$  is the deviation from the (spatial) mean density with respect to its equilibrium value. The relaxation time  $1/K$  for incoming waves should be set so as to guarantee condition (34). According to the analysis of the fluctuation-dissipation balance carried out in the previous section [see Eq. (33)] the relaxation parameter  $K$  should be cast as

$$K = \frac{\nu_L}{(\delta_R \Delta x)^2}. \quad (35)$$

We note that the theoretical approach in Eq. (33) yields  $\delta_R = 1/\sqrt{2} \sim 0.7$ . In order to perform a numerical calibration of the  $K$  parameter an analysis on the mass variance dependence on  $\delta_R$  is required. Figure 3 shows the variance of the mean density  $\langle (\delta \bar{\rho})^2 \rangle$  against  $\delta_R$  for argon at  $\langle \bar{\rho} \rangle = 1.35 \text{ gm/cm}^3$  (which corresponds to an equilibrium density of  $\langle \bar{\rho} \rangle = 0.8 \sigma^{-3}$  in Lennard-Jones units) and temperature  $T = 300 \text{ K}$ . The mesh size is  $\Delta x = 1.377 \text{ nm}$  and the total volume  $V = 3371 \text{ nm}^3$ . The total mass fluctuation increases with  $\delta_R$  (i.e., with the relaxation time  $1/K$ ). According to Fig. 3, for  $\delta_R = 0.4$  the mean density variance coincides with the thermodynamic prescription. This *optimum* value of  $\delta_R$  obtained by numerical means ( $\delta_R = 0.4$ ) differs from the theoretical estimation ( $\delta_R = 0.7$ ), however, as shown below, the predicted form of  $K \propto \nu_L / \Delta x^2$  in Eq. (33) is robust and consistent with the numerical results.

We tested the theoretical prediction  $K = \nu_L / (\delta_R \Delta x)^2$  against a broad range of conditions: varying the mesh size  $\Delta x$  and time step  $\Delta t$ , fluid properties and thermodynamic state, and considering water and argon at several densities.

TABLE I. Results obtained for water and argon at different thermodynamic states, longitudinal kinematic viscosities  $\nu_L$ , and several mesh sizes  $\Delta x$ . A comparison is made between the numerical and theoretical standard deviation of the mean density  $\sigma_{\rho}$ . In all cases we used  $\delta_R=0.4$ .  $V_T$  is the total volume of the system and  $L=397$  nm is the system's size in the  $x$  direction.

| Fluid | $\rho$ (g/cm <sup>3</sup> ) | $T$ (K) | $c$ (m/s) | $\nu_L$ (cm <sup>2</sup> /s) | $\Delta x$ (nm) | $L/\Delta x$ | $V_T$ (nm <sup>3</sup> ) | $\sigma_{\rho_T}^{(num)}$ | $\sigma_{\rho_T}^{(theor)}$ (g/cm <sup>3</sup> ) |
|-------|-----------------------------|---------|-----------|------------------------------|-----------------|--------------|--------------------------|---------------------------|--|
| Water | 1.049                       | 300     | 1467.1    | 0.4560                       | 2.24944         | 60           | 2064.3                   | 0.000939                  | 0.000988   |
| Argon | 1.012                       | 476     | 746.16    | 0.00158                      | 1.37734         | 98           | 3371.8                   | 0.002007                  | 0.001889   |
| Argon | 1.012                       | 300     | 577.72    | 0.00106                      | 1.37734         | 98           | 3371.8                   | 0.001956                  | 0.001923   |
| Argon | 1.012                       | 178.5   | 379.38    | 0.00132                      | 1.37734         | 98           | 3371.8                   | 0.002192                  | 0.002226   |
| Argon | 1.349                       | 300     | 942.15    | 0.00189                      | 1.37734         | 98           | 3371.8                   | 0.001501                  | 0.001366   |
| Argon | 1.349                       | 300     | 942.15    | 0.00189                      | 0.6885          | 196          | 6737.8                   | 0.000875                  | 0.000964   |

Some results for the standard deviation of the total mass of the system are shown in Table I. In all cases considered, the largest relative differences with respect to the thermodynamic value obtained with  $\delta_R=0.4$ , are less than 10%. A finer estimation of the *optimum*  $\delta_R$  provided  $\delta_R=0.40 \pm 0.04$ . We thus conclude that the scheme is robust and that the relaxation parameter  $K$  should be set according to Eq. (35), with  $\delta_R=0.4$  [35]. This is also confirmed by the spectral analysis presented below.

In order to understand how the open boundary works, it is instructive to consider the power-spectral density (PSD) of the local density  $\rho(x, t)$ . The time Fourier-transformed density  $\hat{\rho}(x_i, \omega)$  can be used to evaluate the PSD as,  $S_{\rho}(x_i, \omega) = \langle \hat{\rho}(x_i, \omega, \omega) \hat{\rho}^*(x_i, \omega, \omega) \rangle$ , where  $*$  denotes the complex conjugate. We first discuss the behavior of the spatially averaged PSD,  $\bar{S}_{\rho}(\omega) \equiv (1/N_{cell}) \sum_i S_{\rho}(x_i, \omega)$ , where  $N_{cell}$  is the number of cells in the simulation domain. This function, which is proportional to the dynamic structure function at zero wave number, is shown in Fig. 4, for a set of values of  $\delta_R$ . According to fluctuating hydrodynamics, at equilibrium, fluctuations of all possible wavelengths are equally present in the system and one expects to obtain a flat spectra over a wide band of

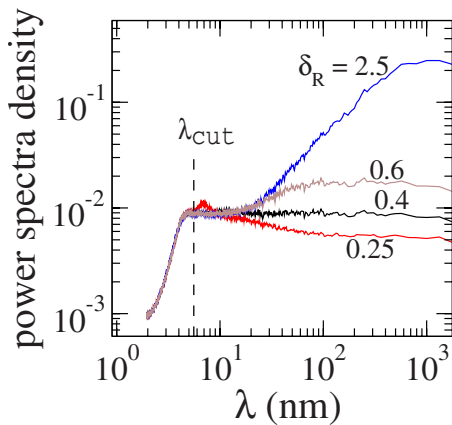


FIG. 4. (Color online) Spatially averaged power spectrum of density,  $\bar{S}_{\rho}(\omega)$ , for liquid argon at  $\rho=1.35$  g/cm<sup>3</sup> and  $T=300$  K vs the wavelength  $\lambda=2\pi c/f$ . The cutoff frequency  $\lambda_{cut}$  is indicated at  $4\Delta x$ . Results correspond to several values of  $\delta_R$ , which determines the relaxation rate  $K=\nu_L/(\delta_R\Delta x)^2$ . The longitudinal viscosity is  $\nu_L=1.9 \cdot 10^{-3}$  cm<sup>2</sup>/s ( $\eta_L=0.25$  cP). The box size is  $L_x=135$  nm and the grid spacing is  $\Delta x=1.377$  nm. The *optimum*  $\delta_R$  corresponds to  $\delta_R=0.4$ .

frequencies. We note, however, that all the spectra resulting from the numerical solution of the FH equations shown in Fig. 4 present a sudden decrease below a cutoff wavelength  $\lambda_{cut} \approx 4\Delta x$ . These short waves are in fact filtered out by the numerical resolution, because from a numerical standpoint one cannot describe a sound wave with less than a few cells.

Figure 4 illustrates how the parameter  $\delta_R$  modifies the spectra of sound waves in the system. Large values of  $\delta_R$  mean small relaxation rates  $K=\nu_L/(\delta_R\Delta x)^2$  for which the “source” of incoming waves is slowly relaxed in time. To better understand the effect of the random generation of incoming waves at the border, one can consider the PSD associated with Eq. (27) given by  $S_{A_1}=\Phi/(K^2+\omega^2)$ . At the long-wavelength range (low frequencies,  $\omega \ll K$ ) the PSD of incoming waves becomes  $S_{A_1} \approx \Phi/K^2 \sim \Phi\delta_R^4$ . This means that the amplitude of the long random waves generated at the boundary decreases with the square of the relaxation time  $1/K^2$  (i.e., with  $\delta_R^4$ ). This can be clearly seen in Fig. 4 where the presence of longer wavelengths is rapidly increased with  $\delta_R$  (see the  $\delta_R=2.5$  case). At the short-wavelength range (high frequencies,  $\omega \gg K$ ) the PSD of incoming waves becomes  $K$  independent,  $S_{A_1} \sim \Phi/\omega^2$ . In agreement with this fact, the low-wavelength region of the spectra in Fig. 4 (which takes into account incoming and outgoing wave contributions) does not greatly vary with  $K$  or  $\delta_R$ . We highlight that, precisely at  $\delta_R=0.4$ , one gets a flat spectrum over the whole range of allowed frequencies (and even for wavelengths much longer than the system size, see Fig. 5).

The mass variance is equal to the integral over the whole frequency range of its power spectral density, thus Fig. 4 clearly indicates that the excess of mass fluctuation observed for large  $\delta_R$  (see Fig. 3) is due to an excess of long-wavelength waves. In the same way, for low values of  $\delta_R$ , long waves are oversuppressed and the total mass of the system becomes too much constrained. In conclusion, an optimum value of the relaxation rate  $K$  is crucial to control the overall mass variance by providing the correct amount of large wavelengths into the system.

#### Comparison with periodic boundaries and rigid walls

One of the objectives of this work is to show that open boundary conditions are required in simulations of phenomena involving the propagation of sound waves. Also, when dealing with fluctuating hydrodynamics, and even at equilib-

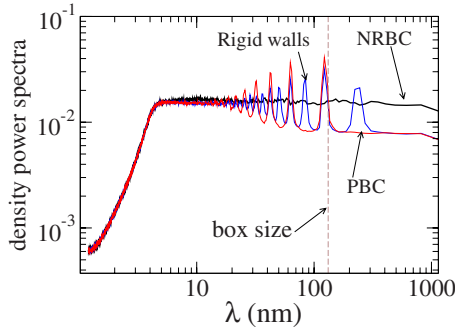


FIG. 5. (Color online) The spatially averaged power spectrum of density  $\bar{S}_\rho(\omega)$  for argon at  $\rho=1.0 \text{ g/cm}^3$  and  $T=300 \text{ K}$ . The simulation domain is  $L_x=135 \text{ nm}$  and  $\Delta x=1.377 \text{ nm}$ . A comparison between NRBCs, PBCs, and rigid walls is made. Frequency  $\omega=2\pi f$  is expressed in wavelength units ( $\lambda=c/f$ ), using the sound velocity  $c=577.7 \text{ m/s}$ .

rium, the stress fluctuations induce sound waves which might become a significant source of momentum, depending on the boundary condition used. In fluid-particle simulations based on the Stokes friction coupling [11], such momentum is transferred to the solute particles, thus generating spurious forces and nonphysical time correlations at sound times. To illustrate this statement, it is quite instructive to compare the sound power spectral densities (at equilibrium) obtained using nonreflecting boundary conditions (NRBCs), periodic boundary conditions (PBC), and rigid walls (RW). Such comparison is illustrated in Fig. 5 for a one-dimensional computational domain of dimension  $L_x=135 \text{ nm}$  and discretized into 98 cells. For PBC and RW, significant peaks are observed at the natural frequencies of the box [ $f_n=nc/L_x$  and  $f_n=nc/(2L_x)$ , respectively]. These peaks become quite large as one approaches the fundamental frequency ( $n=1$ ), corresponding to wavelengths  $\lambda=L_x$  in PBC and  $\lambda=2L_x$  in the RW case (in Fig. 5 we indicate the system size wavelength  $\lambda=L_x$  with a vertical dashed line). The PSD of the velocity exhibits peaks at identical frequencies. As long as the fluid velocity is used for the Stokes force in fluid-particle simulations, these peaks can induce spurious forces to the particles. As shown in Fig. 5, the NRBC formulation avoids finite size effects induced by the eigenfrequencies of the simulation box.

We have not yet discussed how the distribution of sound waves varies at each computational cell. In principle, at equilibrium the distribution should be isotropic and density and velocity at any cell should have similar spectra. In Fig. 6 we show contour plots of the PSD at each cell location,  $S_\rho(x, \omega)$ . In order to facilitate their reading, the frequency  $\omega=2\pi f$  has been expressed in wavelength units  $\lambda=c/f$  and both, position and wavelength, are given in units of the mesh size  $\Delta x$  (i.e.,  $\lambda/\Delta x$  in abscissas and  $x_i/\Delta x$  in ordinates). In the case of NRBCs, the position-dependent PSD  $S_\rho(x, \omega)$  is almost everywhere flat for all wavelengths larger than the cutoff  $\lambda_{cut} \approx 4\Delta x$  (as stated,  $\lambda_{cut}$  corresponds to the limiting wavelength resolved by the mesh). It is worthwhile to mention that the NRBC ensures that the spectra remain flat even for frequencies much larger than the box length (in Fig. 6 we are plotting up to  $\lambda > 10L_x$ ). This nice behavior contrasts with what

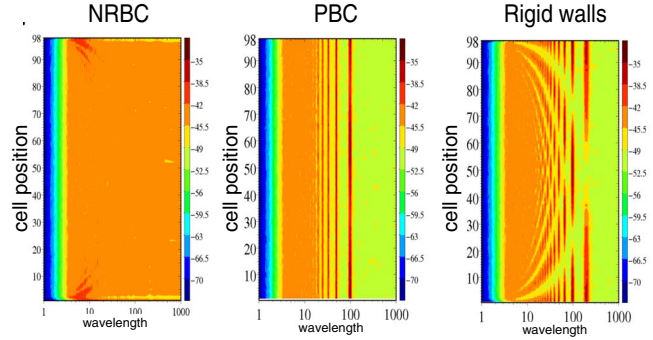


FIG. 6. (Color online) Contour plot of the power spectrum of density at each cell of the domain  $S_\rho(x_i, \omega)$  for the same cases in Fig. 5: NRBCs, PBCs, and rigid walls. The wavelength (abscissas) and the cell position (ordinates) are both given in mesh units  $\Delta x$ . In this unit, the box size is  $L_x/\Delta x=98$ . We note that in the NRBC case, the spectra remains flat even at  $\lambda \gg \lambda_x$ . The thermodynamic equilibrium value is about  $-42 \text{ dB}$ .

was obtained in the periodic and purely reflecting (rigid) walls shown in Fig. 6.

As shown in Fig. 6 the spectra obtained with NRBCs present, however, two small regions near the open boundaries where an excess of short wavelength is observed. The formation of these “boundary layers” is due to the partial reflection of short waves. Indeed, a closer inspection of Fig. 6 shows that the structure of the local maxima of  $S_\rho(x, \lambda)$  at these boundary layers is similar to that produced by purely reflecting rigid walls over the whole spectral range (the reflected waves produce an “echo” whose amplitude has local maxima at  $nx_n=m\lambda_m$ ;  $n$  and  $m$  being integer). The main effect of these reflected waves is to increase the local standard deviation (STD) of density  $\sigma_\rho(x)$  [or velocity  $\sigma_v(x)$ ] near the open boundary, as can be seen in Fig. 7(a). The standard deviation  $\sigma_\rho(x)$  decays exponentially towards its equilibrium value at the bulk  $\sigma_\rho^{eq}$  and thus enables one to obtain a characteristic length  $\delta$ , which is a measure (lower bound) of the thickness of the “reflecting boundary layer” [see the caption of Fig. 7(a)]. Values of  $\delta$  calculated for quite different cases are plotted in Fig. 7(b). Interestingly,  $\delta$  scales with the group  $(c/\nu_L)\Delta x^2$ , which is a measure of the sound absorption length. A wave with wave number  $\lambda$  is damped by viscosity at a rate  $(2\pi^2)\nu_L/\lambda^2$  (the sound absorption coefficient is  $\nu_L/2$ ). Thus, before being damped, reflected waves are able to penetrate back into the domain up to a distance  $\delta_\lambda \approx c\lambda^2/(2\pi^2\nu_L)$ . Inspection of Fig. 6 (for NRBCs) indicates that these reflected waves are shorter than a certain wavelength  $\lambda < \lambda_r$  and that they are responsible for the boundary layer thickness; so one expects  $\delta \sim \delta_{\lambda_r}$ . The trend shown in Fig. 7(b) indicates  $\delta \sim \Delta x^2(c/\nu_L)$ , so one concludes that the reflected wavelengths  $\lambda < \lambda_r$  should only depend on the spatial resolution: this first order estimate yields  $\lambda_r \sim \sqrt{2}\pi\Delta x$ , which is about the spatial resolution limit  $4\Delta x$ . Calculations of the reflection coefficient in Sec. V C confirm this conclusion.

It is interesting to note that, in water, the thickness of the reflecting layer is quite small due to the large viscosity of water ( $\eta_L=4.78 \text{ cP}$ ), which yields  $(c/\nu_L)_{water}=0.4 \text{ nm}^{-1}$ . For instance, for  $\Delta x=2.5 \text{ nm}$ , the reflecting layer remains re-

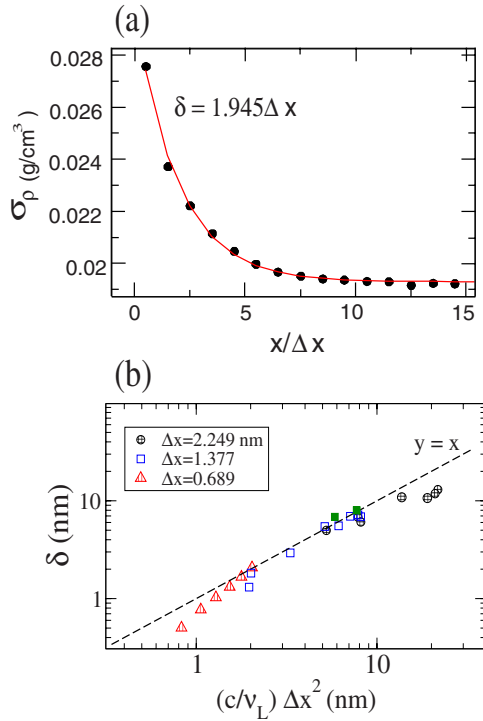


FIG. 7. (Color online) (a) The standard deviation of the density  $\sigma_\rho$  vs the distance from the open boundary  $x$ , for argon at  $\rho_{eq} = 1 \text{ g/cm}^3$ ,  $T=300$ , and  $\Delta x=0.689 \text{ nm}$ . The value of  $\delta$ , measuring the thickness of the reflecting boundary layer, is measured using the fit  $\sigma_\rho(x) = \sigma_\rho^{eq} + A \exp[-x/\delta]$  (solid line), where  $\sigma_\rho^{eq}$  is the equilibrium value and  $A$  is a fitting constant. (b) Values of  $\delta$  against the sound absorption length  $(c/v_L)\Delta x^2$ . The dashed line indicates the order of magnitude estimate  $\delta \sim (c/v_L)\Delta x^2$ . Results were obtained for a system with  $L_x=134.98 \text{ nm}$ , cell volume  $V_c=34.4 \text{ nm}^3$ , and different grid spacing  $\Delta x$ . All results for argon at different densities  $\rho=[0.17-1.34] \text{ g/cm}^3$  and temperatures ( $T=300, 178.5,$  and  $476 \text{ K}$ ).

stricted to the outermost cell. By contrast, in argon at a similar density  $(c/v_L)_{argon}=3.85 \text{ nm}^{-1}$  so the reflecting layer is visible [as in Figs. 6 and 7(a)].

**V. RESULTS**

The results presented in this work are obtained for a 1D implementation of three-dimensional (3D) fluctuating hydrodynamics equations; i.e., we consider 3D cells of volume  $V_c = \Delta x \Delta y \Delta z$ , set up in a 1D array: the number of cells in the  $x$  direction is  $N_x = \{60, 98, 196\}$ , while  $N_y = N_z = 1$ . We also carried out tests for 2D and 3D flows, which will be presented in a future work, along with a more detailed explanation of the adaptation of the staggered scheme to the FH equations, outlined in Appendix A.

**A. Equilibrium**

Several tests at equilibrium are first required when presenting a fluctuating hydrodynamics solver. Figure 8 shows the standard deviation of the density at one fluid cell, obtained for argon, ranging from gas to liquid. Deviations from

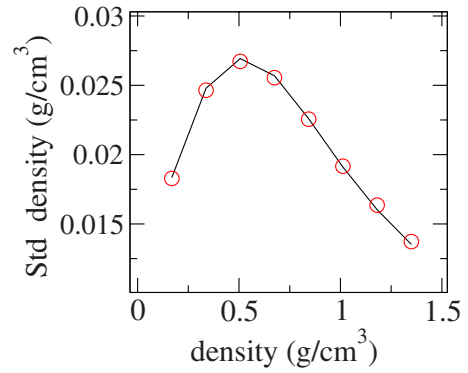


FIG. 8. (Color online) Standard deviation of the density at one grid cell located in the center computational domain with volume  $V_c=34.4 \text{ nm}^3$  vs the mean density of the system. Results were obtained for argon an equation of state at  $T=300 \text{ K}$ , using  $L_x=135 \text{ nm}$  and  $\Delta x=0.688 \text{ nm}$ . A solid line indicates the expected thermodynamic value.

the thermodynamic prescription (solid line) are negligibly small. Figure 9 shows the kinetic temperature (output temperature)  $T_o$  and the standard deviation of density  $\sigma_\rho$  at each fluid cell. Results correspond to the water model. The kinetic temperature is related to the velocity variance,  $\sigma_v^2$  via  $k_B T_o = \sigma_v^2 \langle \rho \rangle V_c$ , where  $\sigma_v$  and  $\langle \rho \rangle$  are local cell quantities and  $V_c$  is

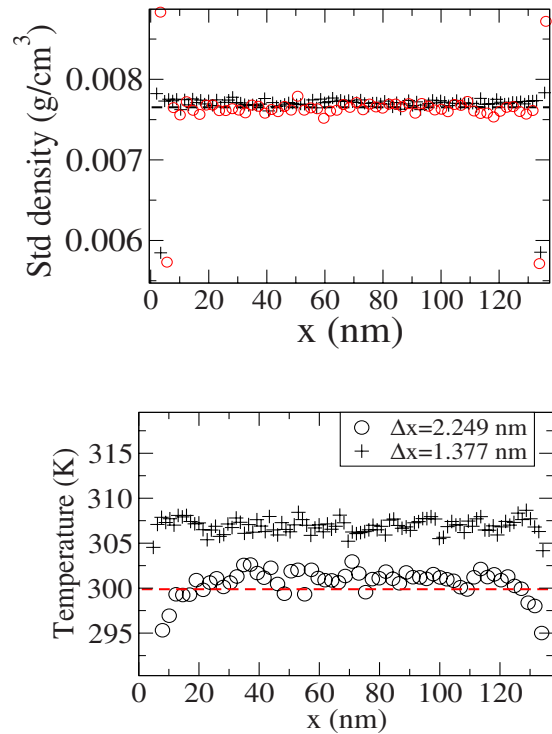


FIG. 9. (Color online) The standard deviation of density and the kinetic (output) temperature  $T_o = \langle \rho V_c \rangle \sigma_v^2 / K_B$  vs the cell position in an equilibrium calculation using the water model. The dashed lines show the thermodynamic value at the prescribed temperature  $T = 300 \text{ K}$ . The standard deviation of velocity  $\sigma_v$  differs with respect to the thermodynamic value in less than 1% for  $\Delta x=2.249 \text{ nm}$  and about 2.3% for  $\Delta x=1.377 \text{ nm}$ . Density fluctuations are in very good agreement with the theoretical value.

the fixed cell volume. We found deviations from the “input” temperature of a few percent (see the caption of Fig. 9, where the imposed temperature is  $T=300$  K).

The sudden jump of  $T_o$  and  $\sigma_\rho$  near the boundaries observed in Fig. 9, is due to the reflection of short waves. However, as discussed above, in the case of water the width of the reflective boundary layer is quite small (about  $\Delta x$ ). The distribution of velocity and density fluctuations is flat along most of the system and, only the first and second cell adjacent to the boundary deviate from the bulk behavior. As stated before, in the case of argon  $\sigma_v(x)$  and  $\sigma_\rho(x)$  converge exponentially to the thermodynamic value at the bulk [see Fig. 7(a)]. The STD at the boundaries are typically about 1.4 times larger than within the bulk.

### B. Periodic forcing

Another set of tests for the open boundary conditions comprise forcing of sound waves inside the channel. We shall first compare the results obtained using NRBCs and periodic boundaries and then calculate the reflection coefficient in our NRBC formulation.

Forcing of waves inside the channel can be done in several ways. For instance, if the objective is to introduce harmonic waves from the *west* boundary (i.e., waves moving rightwise), one can add a sinusoidal term into the  $A_5$  amplitude equation (21).

$$L_5^{(f)} = L_5 + a_{L_5} \cos(\omega_f t), \quad (36)$$

where  $L_5^{(f)}$  is the modified  $L_5$ ,  $a_{L_5}$  is proportional to the amplitude of the forced incoming waves, and  $\omega_f$  is the forcing (angular) frequency.

Alternatively, it is also possible to add a sinusoidal force (or some mass production term) to the momentum (or density) equation at some cell in the bulk. Both procedures provide similar results; the following tests were done by adding an oscillatory mass source production term in the continuity equation at  $x=x_f$ ,

$$\frac{\partial \rho(x_f, t)}{\partial t} = -\frac{\partial \rho u}{\partial x} + a_\rho \sin(\omega_f t). \quad (37)$$

The latter procedure is useful to study the reflection of short waves because they are damped at such a high rate that their amplitude becomes smaller than thermal noise at relatively short distances from their source. To ensure a significant signal to noise ratio in the study of reflection, we placed the wave source  $x_f$  at a distance  $x_f = \lambda_f + 5\Delta x$ , where  $\lambda_f$  is the wavelength of the forced wave.

Figure 10 compares the spatially dependent power spectra [as a function of the wavelength,  $S_\rho(x, \lambda)$ ] obtained when forcing waves inside the channel at a certain frequency  $\omega_f = 2\pi c/\lambda_f$  and using either NRBCs or PBCs. The difference is clear; while in the NRBC case a well defined peak with similar amplitude at every cell of the system is obtained at the forcing frequency  $\omega_f$  in the PBC case, one gets a complicated  $x$ -dependent pattern at the forcing frequency. This pattern is essentially determined by a standing wave that interferes with the eigenwaves of the simulation box at frequencies  $\omega_n = 2\pi n c/L$ .

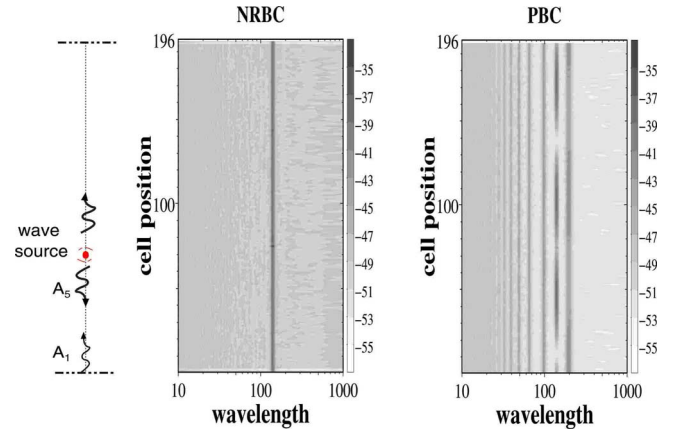


FIG. 10. (Color online) Contour plot showing the PSD of the density (in dB) at each cell, under an sinusoidal forcing with wavelength  $\lambda_f = 496.32$  nm ( $\lambda_f/\Delta x = 135$ ), induced at cell #75. Wavelength  $\lambda$  and cell positions are given in units of  $\Delta x = 0.688$  nm. The sound frequency (in Hz) is  $f = c/\lambda$ , where  $c = 942.16$  m/s is the sound velocity. Results were obtained for argon at  $\rho = 1.34$  g/cm<sup>3</sup> and  $T = 300$  K. A comparison is made between NRBCs and PBC. The leftmost figure depicts the setup used: a wave source (red circle) impinges sound waves ( $A_5$ ) in both senses; the reflected wave ( $A_1$ ) is measured at the bottom ( $x=0$ ) boundary.

### C. Reflection coefficient

Figure 11 shows the reflection coefficient obtained using the forcing procedure described above. The reflection coefficient is obtained from the ratio  $r = \hat{A}_1/\hat{A}_5$  between the amplitude of the outgoing (imposed) wave  $\hat{A}_5$  and the incoming wave  $\hat{A}_1$  (resulting from any partial reflection). The amplitude of the waves was evaluated at some cells near the  $x_b = 0$  boundary, from the magnitude of the maximum peak in their Fourier spectra (i.e., at the forcing frequency  $\omega_f$ )  $\hat{A}_i^2 = S_{A_i}(x_o, \omega_f)$ . The “test” cells  $x_o$  are placed between the open boundary and the location of the wave source:  $x_b < x_o < x_f$ .

Values of the reflection coefficient are shown in Fig. 11. We note that the values of  $r$  obtained from deterministic hydrodynamics (i.e., switching off fluctuations) were found to be similar to those obtained from the fluctuating case. In fact, results for  $r$  reported by Polifke *et al.* [30] for large eddy simulations of turbulent flow [also included in Fig. 11(a)] are consistent with our laminar flow calculations indicating that the behavior of  $r$  with  $f$  does not greatly depend on fluctuations, flow or fluid conditions, but rather on the numerical resolution used. In particular, as shown in Fig. 11(a), waves with short enough wavelength are partially reflected: we find that irrespective of the fluid properties or flow (fluctuations) conditions,  $r \approx 0.5$  for  $\lambda < \lambda_r$  with  $\lambda_r \sim 10\Delta x$ . This threshold for partial reflection agrees with the estimation done in Sec. IV and it can be clearly seen in the NRBC case of Fig. 6. Larger wavelengths present a rapid decrease of their reflection coefficient. Our results fit with the trend  $r \sim 10^{-3}(f\Delta x)^{1.5}$ , shown by the dashed line in Fig. 11(b). However, the behavior of  $r$  at low frequencies obtained by Polifke *et al.* for turbulent flow scales with a smaller slope  $r \sim f^{0.95}$ , suggesting that the type of flow might

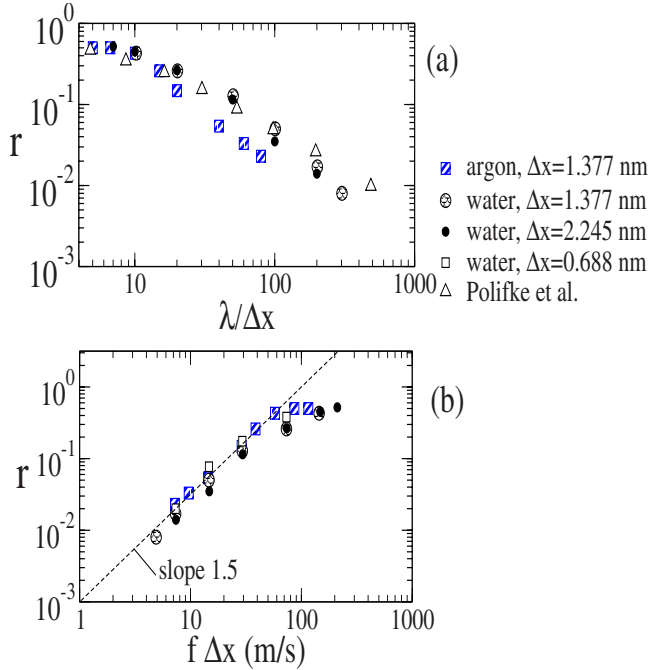


FIG. 11. (Color online) The reflection coefficient  $r$  calculated as the ratio between maximum amplitudes of the reflected and forced wave  $r = \hat{A}_1^{\max} / \hat{A}_5^{\max}$ . Results correspond to liquid argon at  $\rho = 1.0 \text{ g/cm}^3$  and water (both at  $T=300 \text{ K}$ ), whose sound velocities are  $c_{\text{argon}}=577.7 \text{ m/s}$  and  $c_{\text{water}}=1480 \text{ m/s}$ . Results obtained by Polifke *et al.* [30] from large eddy simulation of turbulent flow have also been included. (a) The reflection coefficient vs the nondimensional wavelength  $\lambda/\Delta x$  and (b) vs the group  $f\Delta x$ , where  $f=\lambda/c$  is the frequency in Hz. The dashed line corresponds to the best fit to our results  $r \approx 10^{-3}(f\Delta x)^{1.5}$ .

have some effect on  $r$  at low frequencies. We note that the energy of the reflected wave decreases like  $r^2$  so values of  $r \sim 0.1$  can be already sought as nonreflecting. In this sense, the trend  $r \approx 10^{-3}(f\Delta x)^{1.5}$  is useful to estimate the spatial resolution ( $\Delta x$ ) ensuring evacuation of a given frequency:  $f\Delta x \approx 20 \text{ m/s}$  for  $r \approx 0.1$ .

## VI. CONCLUSIONS

We have presented a formalism for NRBCs, which allows one to evacuate sound waves out of an open fluid domain described by fluctuating hydrodynamics. This set of open boundary conditions, originally derived for standard CFD, consists of solving the linearized Navier-Stokes equations at the open boundary, in the normal-to-boundary direction. A key difference, when dealing with fluctuating hydrodynamics, is the fact that we are considering very small volumes of fluid where mass fluctuations are significant. Therefore, the NRBC formalism should enable the exchange of mass between the computational domain and its surroundings, arising from longitudinal stress fluctuations. These fluctuations are reflected in the variance of the total mass and momentum of the system whose values at equilibrium are prescribed by the grand canonical ensemble thermodynamics. Thus, the purpose of the NRBC in fluctuating hydrodynamics is two-

fold: first, to evacuate large amplitude sound waves and second, to drive the system to the proper thermodynamical equilibrium. These two requirements are met by a stochastic equation for the amplitude of the incoming waves, which needs to be postulated in the NRBC formalism. On one hand, the deterministic part of this boundary equation ensures the so-called “plane-wave masking” [30], which avoids the reflection of sound waves with amplitudes larger than the thermal noise. On the other hand, the random stress near the boundary acts as a source of random waves into the system. By including the longitudinal stress fluctuations into the boundary equation analysis, we could derive a fluctuation-dissipation balance for the incoming waves amplitude which takes into account the thermodynamic equilibrium conditions to fit the only free parameter of the system: the relaxation rate of the incoming waves,  $K$ . We obtained  $K = \nu_L / (\delta_r \Delta x)^2$ , where  $\nu_L$  is the longitudinal kinematic viscosity of the fluid,  $\Delta x$  is the computational cell size and  $\delta_r$  is a nondimensional length. We show that  $\delta_r = 0.4$  provides the correct total mass variance regardless of the fluid properties and mesh resolution. An interesting outcome is that the relaxation rate  $K$  actually controls the power spectra of density and momentum inside the entire system; this might be useful to tune the sound power spectra in other types of scenarios, such as turbulence.

The present method avoids some of the finite size effects induced by periodic boundaries in fluid-particle simulations and more importantly it provides a useful tool for the simulation of problems involving the propagation of sound waves, such as the design of ultrasound devices or the study of nanoparticle-ultrasound interaction.

## ACKNOWLEDGMENTS

Both authors benefit from the Ministerio de Educación y Ciencia “Ramón y Cajal” research contract, funded by the Spanish government. R.D.-B. acknowledges funding from Project No. FIS2007-65869-C03-01. Part of this work was carried out at the Dept. CC.TT. Fisicoquímicas, UNED (Madrid), funded by the Marie-Curie European Reintegration Grant No. MERG-CT-2004-006316. The authors are grateful to the UNED department’s personnel for their help.

## APPENDIX A: FLUCTUATING HYDRODYNAMICS IN A STAGGERED GRID

The finite volume method is used to solve the fluctuating Navier-Stokes equations. Spatial gradients are discretized using centered differences and time integration is done by a fully explicit Euler scheme. The time step was set to  $\Delta t \approx 10 \text{ fs}$ , yielding a Courant number  $c\Delta t/\Delta x \sim 0.01$ , similar to those used in previous works [20,36]. The Euler scheme requires relatively small time steps to keep thermodynamic consistency for density fluctuations and also to recover proper hydrodynamics. An accuracy test, similar to that presented in Ref. [20], showed that the time autocorrelation of short-wavelength modes is correct up to the spatial resolution limit  $\sim 5\Delta x$ . In passing, we note that it is possible to increase  $\Delta t$  by using more elaborate time integration

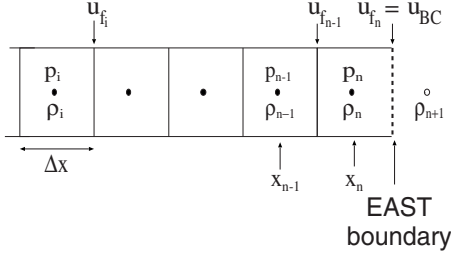


FIG. 12. Staggered grid scheme near the east boundary.

schemes [36]. Most of the previous works on fluctuating hydrodynamics [19,20,36] have implemented their numerical scheme in a collocated grid, whereby all the set of flow variables are resolved at the same position of each volume cell: its center. In this work we have implemented a staggered grid for fluctuating hydrodynamics. The staggered arrangement is illustrated in Fig. 12. Each scalar variable (density and pressure in our case) is computed at the cell centers while the velocity components are resolved at the cell faces. A previous work by Garcia *et al.* [37] made use of a staggered grid arrangement wherein velocity and temperature were resolved at the integration cell faces and density at the integration cell centers in the aim to well define the boundary condition on the mass flux.

Compared to a collocated grid, the staggered grid used here provides a much better coupling between the pressure and velocity field. This results in several advantages: first, it avoids the formation of numerical pressure and velocity oscillations (see Patankar [38]) and second, the boundary conditions are well defined. In the staggered arrangement one requires an explicit boundary condition for the velocity and density but there is no need of defining an extra boundary condition for the pressure. In any case, the NRBC formulation can be also applied in collocated (both regular or unstructured) grids and even for turbulent flows (see, e.g., [9]).

We briefly describe the discrete operators involved in a finite volume formulation applied to a staggered grid arrangement; details can be found in Ref. [38]. Conservation equations can be cast in the general form

$$\frac{\partial \rho \Phi}{\partial t} = -\nabla \cdot (\rho \mathbf{u} \Phi - \mathbf{J}_\Phi), \quad (\text{A1})$$

where  $\Phi=1$  for mass and  $\Phi=\mathbf{u}$  for momentum conservation equations. In the mass equation  $\mathbf{J}_1=0$ , while  $\mathbf{J}_u=(p\mathbf{1}+\mathbf{\Pi})$  is the pressure tensor appearing in the momentum equation. The conservation equations (A1) are integrated over control cells of volume  $V$ . By integrating Eq. (A1) and applying the Gauss theorem to the convection and gradient terms, one gets

$$V \frac{(\rho_c \Phi_c)^k - (\rho_c \Phi_c)^{k-1}}{\Delta t} = - \sum_f (\rho_f \mathbf{u}_f \cdot \mathbf{S}_f \Phi_f - [\mathbf{J}_\Phi]_f \cdot \mathbf{S}_f)^{k-1}. \quad (\text{A2})$$

The cell center of the integration volume in the above equations is noted by the subscript  $c$ , while  $f$  stands for the face of the integration domain. Superscript “ $k$ ” in Eq. (A2) refers

to the integration time  $t_k=k\Delta t$  and the face area (normal vector) is  $\mathbf{S}_f$ .

As stated, in the staggered grid arrangement the scalar variables (density and pressure) are resolved at the volume cell center while the velocity vector components are defined at the cell faces (we actually solve the momentum equation using the velocity as the primitive variable). To be consistent with this choice, as shown in Fig. 12, the centers of the control cells for the mass equation are placed at the volume cell centers, i.e.,  $c \rightarrow x_i$  in Eq. (A2). In the momentum equation the center of the integration volume is located at the cell faces; i.e.,  $c \rightarrow x_i + \Delta x/2$  in Eq. (A2). As an example, in one dimension, the mass equation is integrated over  $x_i - \Delta x/2 \leq x \leq x_i + \Delta x/2$ , while the momentum equation is integrated over  $x_i \leq x \leq x_{i+1}$ . Whenever necessary variables are interpolated, as done in the standard finite volume method [38]: for instance, the computation in the mass equation of the flux at the face located at  $x_i + \Delta x/2$ ; is calculated as  $\rho_f u_f = 0.5(\rho_i + \rho_{i+1})u_f$ .

## APPENDIX B: NONREFLECTING BOUNDARY CONDITIONS

For completeness we first describe the implementation of periodic boundaries and rigid walls. At the west boundary, periodic boundary conditions imply  $\rho_0=\rho_n$  and  $u_{f_0}=u_{f_n}$ , while at the east boundary,  $\rho_{n+1}=\rho_1$  and  $u_{n+1}=u_1$ . *Rigid wall boundary conditions* are implemented as  $\rho_0=\rho_1$  and  $u_{f_0}=0$  at the west boundary and  $\rho_{n+1}=\rho_n$  and  $u_{f_n}=0$  at the east boundary. A benefit of the staggered grid arrangement is that boundary conditions on the pressure are not required.

Let us now focus on the implementation of the *nonreflecting boundaries*. We first deal with the east outflow boundary. The relations giving the time variation amplitudes  $L_5$  and  $L_1$  [see Eqs. (11) and (14)] are discretized at the first face cell located upward of the outflow boundary, i.e., at  $x_{n-1} + \Delta x/2$  (see Fig. 12); so that the discretized relations take the form

$$L_5 = \lambda_5 \left( \frac{p_n - p_{n-1}}{\Delta x} + \rho_e c \frac{u_n - u_{n-1}}{\Delta x} \right), \quad \lambda_5 = u_{f_{n-1}} + c, \quad (\text{B1})$$

where  $\rho_n, \rho_{n-1}, p_n, p_{n-1}, u_n$ , and  $u_{n-1}$  are the values taken at the cell centers located at  $x_n$  and  $x_{n-1}$ , for the density, pressure, and velocity, respectively. Due to the staggered grid arrangement, the velocities  $u_n$  and  $u_{n-1}$  have to be interpolated, this is done by a simple linear interpolation.

$$u_n = \frac{1}{2}(u_{BC} + u_{f_{n-1}}) \quad \text{and} \quad u_{n-1} = \frac{1}{2}(u_{f_{n-1}} + u_{f_{n-2}}). \quad (\text{B2})$$

The time amplitude variation,  $L_1$  [see Eq. (25)], is also computed at the first face,  $x_{n-1} + \Delta x/2$ , upwards the outflow boundary condition, so that

$$L_1 = K \rho_e c A_1, \quad (\text{B3})$$

where

$$A_1 = \frac{1}{2} \left( \frac{p_{f_{n-1}} - p_e}{\rho_e c} - u_{f_{n-1}} \right), \quad (\text{B4})$$

where  $p_{f_{n-1}}$  is the pressure interpolated at the face cell  $n-1$  given by  $p_{f_{n-1}} = (p_n + p_{n-1})/2$ .

The velocity at the border  $u_{BC}$  is solved from numerical integration of Eq. (18), using a Euler scheme,

$$u_{BC}^{t+\Delta t} = u_{BC}^t - \frac{\Delta t}{2\rho_e c} (L_5^t + L_1^t). \quad (\text{B5})$$

The density at the boundary  $\rho_{BC}$  could be, in principle, obtained from time integration of Eq. (16). However, we found that the solution of Eq. (16) leads to numerical instability. Instead, we used an equivalent formulation of the LODI equations based on the spatial gradient at the border (see Ref. [7]),

$$\left( \frac{\partial \rho}{\partial x} \right)_{BC} = \frac{1}{c^2} \left[ \frac{L_2}{\lambda_2} + \frac{1}{2} \left( \frac{L_5}{\lambda_5} + \frac{L_1}{\lambda_1} \right) \right], \quad (\text{B6})$$

where  $\lambda_i$  are given by Eq. (15) (with  $u$  also measured at the  $f-1$  face), and the whole right-hand side of Eq. (B6) is measured at time  $t$ . We note that in the present work heat is not included so that  $L_2=0$ .

By defining  $\rho_{n+1}$  as the density at the ghost cell  $n+1$  [required to define  $\rho_{BC}$  and  $(\partial \rho / \partial x)_{BC}$ ], the density value at the east frontier of the domain is given as follows:

$$\rho_{n+1} = \rho_n + \left( \frac{\partial \rho}{\partial x} \right)_{BC} \Delta x. \quad (\text{B7})$$

At equilibrium and low Reynolds number calculations considered here, the density gradient at the boundary was found to be negligibly small. In practice, the zero mass flux condition,

$$\rho_{n+1} = \rho_n \quad (\rho_{BC} = \rho_n) \quad (\text{B8})$$

was found to provide similar results to Eq. (B7).

For the derivation of the open boundary condition at the west border of the computational domain, one needs to note that the outgoing waves now correspond to the amplitudes  $A_5$  and the incoming wave to  $A_1$ . Also, one needs to take into account that the  $x$  axis is reversed. The variation of the outgoing wave is thus computed from

$$L_1 = -\lambda_1 \left( \frac{p_2 - p_1}{\Delta x} - \rho_e c \frac{u_2 - u_1}{\Delta x} \right), \quad \lambda_1 = u_{f_1} - c, \quad (\text{B9})$$

while the incoming wave variation is approximated by

$$L_5 = -K \rho_e c A_5, \quad (\text{B10})$$

with

$$A_5 = \frac{1}{2} \left( \frac{p_{f_1} - p_e}{\rho_e c} + u_{f_1} \right). \quad (\text{B11})$$

$u_1$ ,  $u_2$ , and  $p_{f_1}$  are estimated by linear interpolation.

- 
- [1] L. D. Landau and E. M. Lifshitz, *Fluid Mechanics* (Pergamon Press, New York, 1959).
- [2] J. Keizer, *Statistical Thermodynamics of Non-Equilibrium Processes* (Springer-Verlag, New York, 1987).
- [3] J. Christensen, A. I. Fernandez-Dominguez, F. Leon-Perez, L. Martin-Moreno, and F. J. Garcia-Vidal, *Nat. Phys.* **3**, 851 (2007).
- [4] A. Haake and J. Dual, *J. Acoust. Soc. Am.* **117**, 2752 (2005).
- [5] J. A. Cosgrove, J. M. Buick, D. M. Campbella, and C. A. Greated, *Ultrasonics* **43**, 21 (2004).
- [6] T. J. Poinso and S. K. Lele, *J. Comput. Phys.* **101**, 104 (1991).
- [7] T. Poinso and D. Veynante, *Theoretical and Numerical Combustion*, 2nd ed. (Edwards, Ann Arbor, 2005).
- [8] T. Colonius, *Annu. Rev. Fluid Mech.* **36**, 315 (2004).
- [9] L. Selle, G. Lartigue, T. Poinso, R. Koch, K. U. Schildmacher, W. Krebs, B. Prade, P. Kaufmann, and D. Veynante, *Combust. Flame* **137**, 489 (2004).
- [10] O. Berk Usta, Anthony J. C. Ladd, and Jason E. Butler, *J. Chem. Phys.* **122**, 094902 (2005).
- [11] G. Giupponi, G. De Fabritiis, and P. V. Coveney, *J. Chem. Phys.* **126**, 154903 (2007).
- [12] R. Adhikari, K. Stratford, M. E. Cates, and A. J. Wagner, *Europhys. Lett.* **71**, 473 (2005).
- [13] S. Williams, J. B. Bell, and A. L. Garcia, *SIAM Multiscale Modeling and Simulation* **6**, 1256 (2008).
- [14] G. De Fabritiis, R. Delgado-Buscalioni, and P. Coveney, *Phys. Rev. Lett.* **97**, 134501 (2006).
- [15] R. Delgado-Buscalioni and G. De Fabritiis, *Phys. Rev. E* **76**, 036709 (2007).
- [16] R. Delgado-Buscalioni, *Phys. Rev. Lett.* **96**, 088303 (2006).
- [17] A. Donev, A. L. Garcia, and B. J. Alder, *J. Comput. Phys.* **227**, 2644 (2008).
- [18] R. Delgado-Buscalioni, P. V. Coveney, and G. De Fabritiis, *Proc. Inst. Mech. Eng., Part C: J. Mech. Eng. Sci.* **222**, 769 (2008).
- [19] M. Serrano and P. Español, *Phys. Rev. E* **64**, 046115 (2001).
- [20] G. De Fabritiis, M. Serrano, R. Delgado-Buscalioni, and P. V. Coveney, *Phys. Rev. E* **75**, 026307 (2007).
- [21] K. Johnson, J. A. Zollweg, and K. E. Gubbins, *Mol. Phys.* **78**, 591 (1993).
- [22] D. M. Heyes, *Chem. Phys. Lett.* **153**, 319 (1988).
- [23] G. W. Hedstrom, *J. Comput. Phys.* **30**, 222 (1979).
- [24] K. W. Thompson, *J. Comput. Phys.* **68**, 1 (1987).
- [25] Jean Pierre Boon and Sidney Yip, *Molecular Hydrodynamics* (Dover Publications, New York, 1992).
- [26] J. C. Strikwerda, *Commun. Pure Appl. Math.* **30**, 797 (1977).
- [27] J. Olinger and A. Sundstrom, *SIAM J. Appl. Math.* **35**, 419 (1978).
- [28] D. H. Rudy and J. C. Strikwerda, *J. Comput. Phys.* **36**, 55 (1980).
- [29] L. Selle, F. Nicoud, and T. Poinso, *AIAA J.* **42**, 958 (2004).
- [30] W. Polifke and P. Moin C. Wall, *J. Comput. Phys.* **213**, 437 (2006).
- [31] By making use of Eq. (23), it is possible to calculate the re-

- flection coefficient  $R(\omega)=A_1/A_5$  [30], which takes the form  $r(\omega)=K/(K^2+4\omega^2)^{(1/2)}$ , where  $\omega$  is the wave angular frequency.
- [32] The formal resolution of the FD balance for a nonreflecting boundary is a complicated task because it would require consideration of Eqs. (17) and (18) as the boundary conditions to the fluctuating Navier-Stokes equations, inside the domain.
- [33] N. C. Nigam, *Introduction to Random Vibrations (Structural Mechanics)* (MIT Press, Boston, USA, 1983).
- [34] For arbitrary  $\gamma$  one has  $A_1=(1/2)[\delta p/(\rho_e c_S)-\delta u]$ ,  $\langle \delta p^2 \rangle = c_T^2 c_S^2 \langle \delta \rho^2 \rangle$ , and  $\langle \delta \rho^2 \rangle = \rho_e k_B T / (c_T^2 V_c)$ , where  $c_T$  and  $c_S$  are the isothermal and adiabatic sound velocities ( $c_S^2 = \gamma c_T^2$ ). These relations lead to the same result of Eq. (32).
- [35] The optimum value of  $\delta_R$  might slightly vary if using different discretization, such as a collocated scheme.
- [36] J. B. Bell, A. L. Garcia, and S. A. Williams, *Phys. Rev. E* **76**, 016708 (2007).
- [37] A. L. Garcia, M. M. Mansour, G. C. Lie, and E. Clementi, *J. Stat. Phys.* **47**, 209 (1987).
- [38] S. V. Patankar, *Numerical Heat Transfer and Fluid Flow* (Hemisphere Publishing Corporation, New York, 1980).